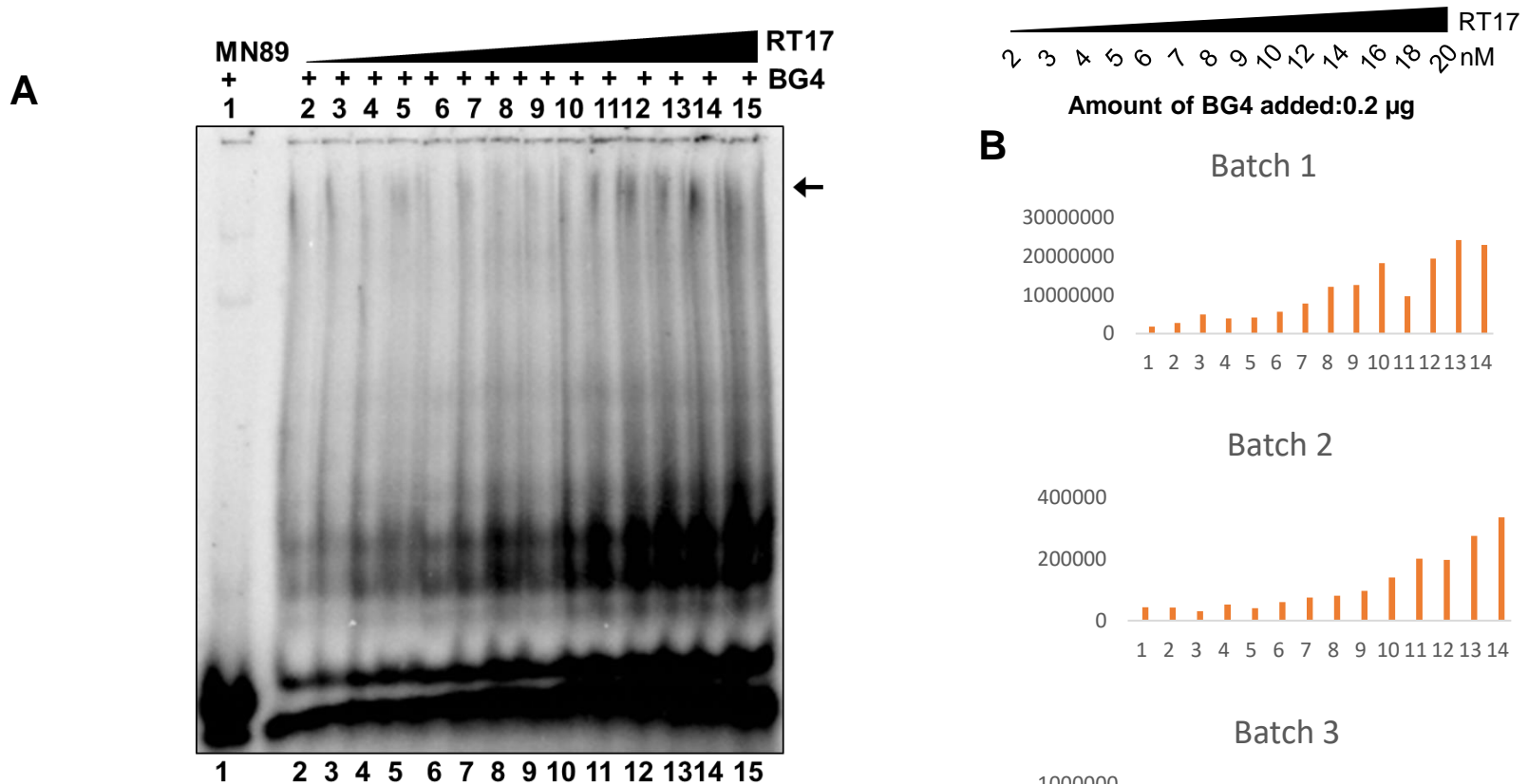
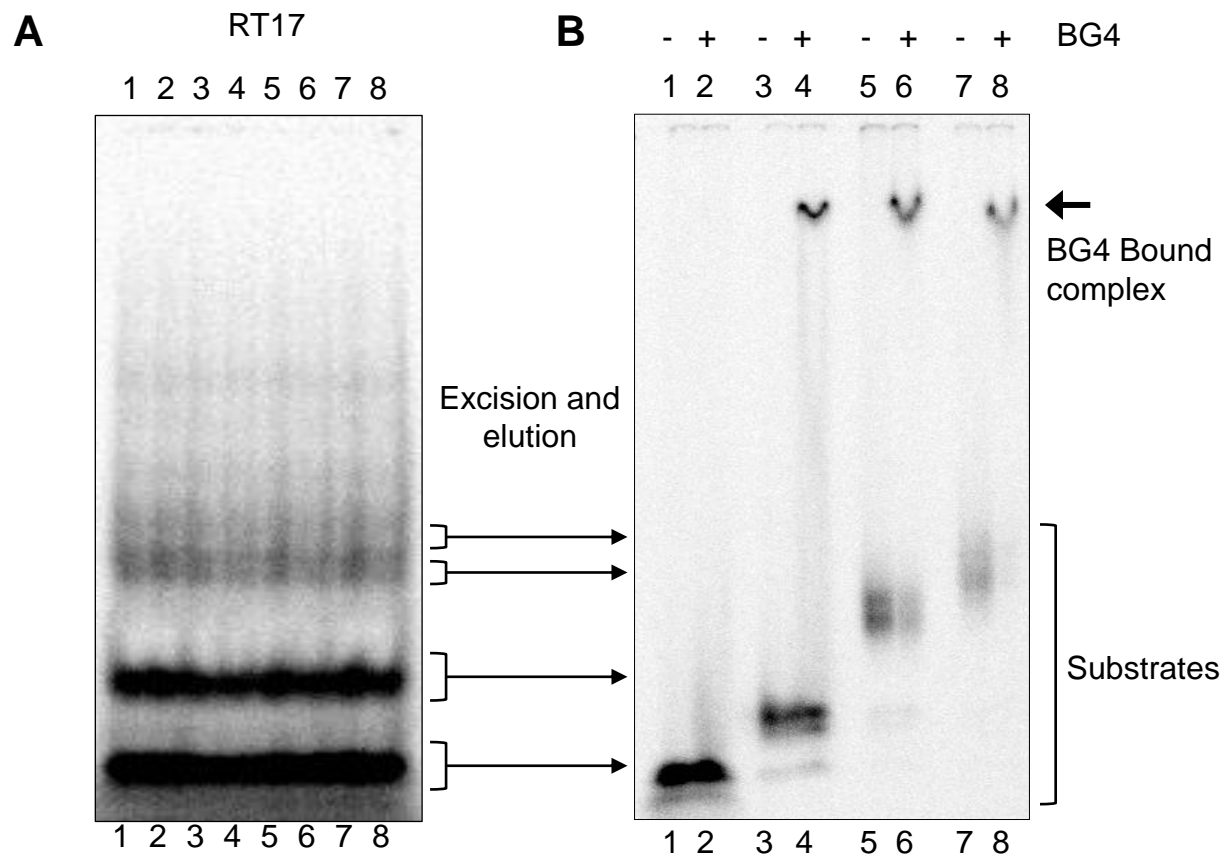


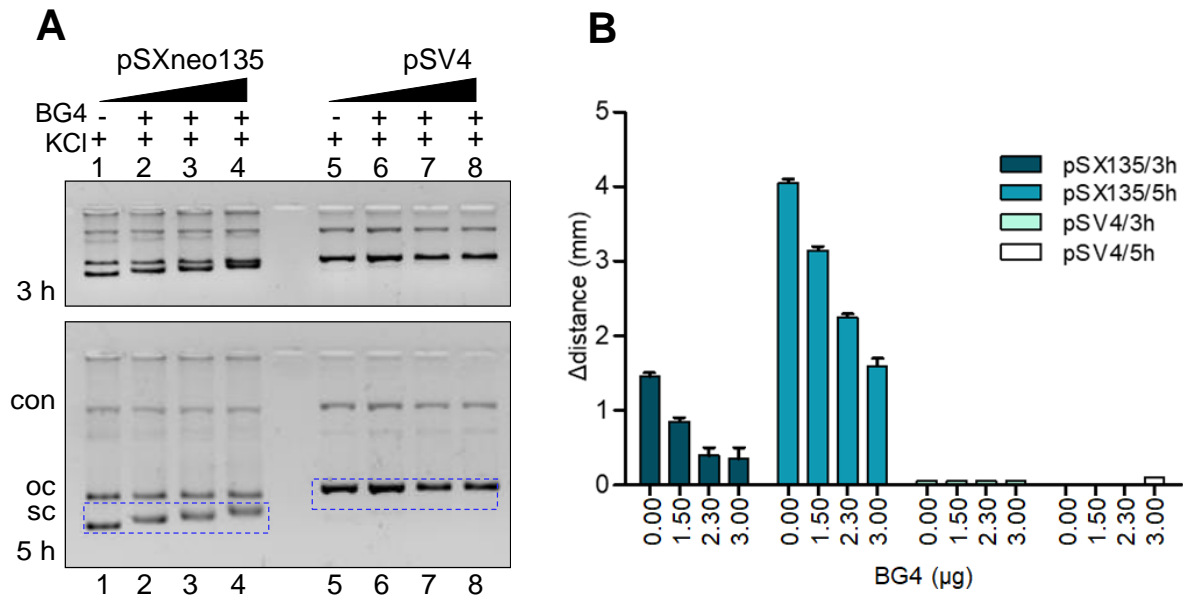
Supplementary Figure 1. Purification of BG4 antibody and evaluation of its purity and activity. **A.** BG4 antibody was expressed in *E. coli* BL21(DE3) using pSANG10-3F-BG4 and subjected to Ni-NTA affinity chromatography and different fractions were evaluated. Imidazole eluted fractions were resolved on SDS-PAGE, stained with Coomassie and purity of BG4 was compared. M is molecular weight ladder. **B.** Western blotting to confirm identity of purified fraction. Ponceau stained membrane is also shown to indicate molecular weight. **C.** Gel mobility shift assay showing BG4 binding to G-quadruplex DNA. BG4 binding activity of purified fractions was assessed by incubating (37°C) radiolabelled G4 forming sequence of *Hif1 α* , RT17 with different batches of BG4 antibody (lanes 5-10). The products were resolved on a 6% native polyacrylamide gel containing KCl. Complementary sequence, C-rich DNA, MN89, was also incubated and loaded as control (lanes 1, 2). Band due to BG4 binding is indicated with an arrow. **D.** Bi-layer interferometry sensorgrams depict the real-time binding of BG4 to 5' biotinylated oligomer derived from *Hif1 α* substrate that is immobilised to SSA sensors. Sensorgram curves depict the association, followed by dissociation of increasing concentrations of antibody to the sensors. Real time binding curves helped calculate equilibrium dissociation constant (K_d) by globally fitting the rate equation for 1:1 kinetics to data. Dissociation constant (K_d) value of BG4 for *Hif1 α* is 17.4 ± 0.588 nM.



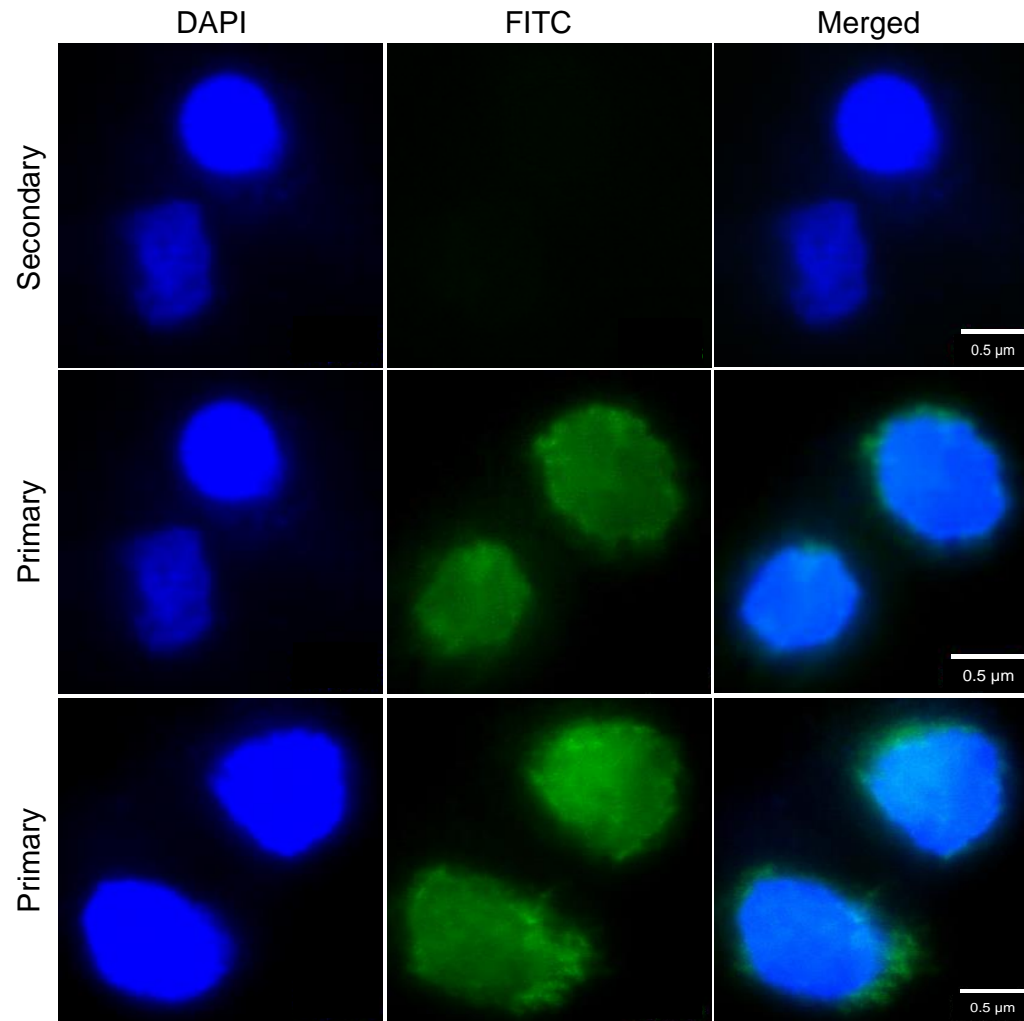
Supplementary Figure 2. Substrate titration of RT17 with BG4 antibody. **A.** Gel image showing binding of BG4 (0.2 µg) to G4-DNA (RT17). Radiolabelled Hif1α oligomeric substrate, RT17 (lanes 2– 15), was incubated in 100 mM KCl at 37°C in increasing concentrations (2, 3, 4, 5, 6, 7, 8, 9, 10, 12, 14, 16, 18, 20 nM), followed by incubation with BG4 at 4°C. Bound DNA (indicated by an arrow) was then electrophoresed on 6% native polyacrylamide gel. Complementary C-rich sequence, MN89, fails to show any binding (lane 1). **B.** Bar diagram showing increase in formation of bound complex with an increase in RT17 concentration ($p < 0.05$).



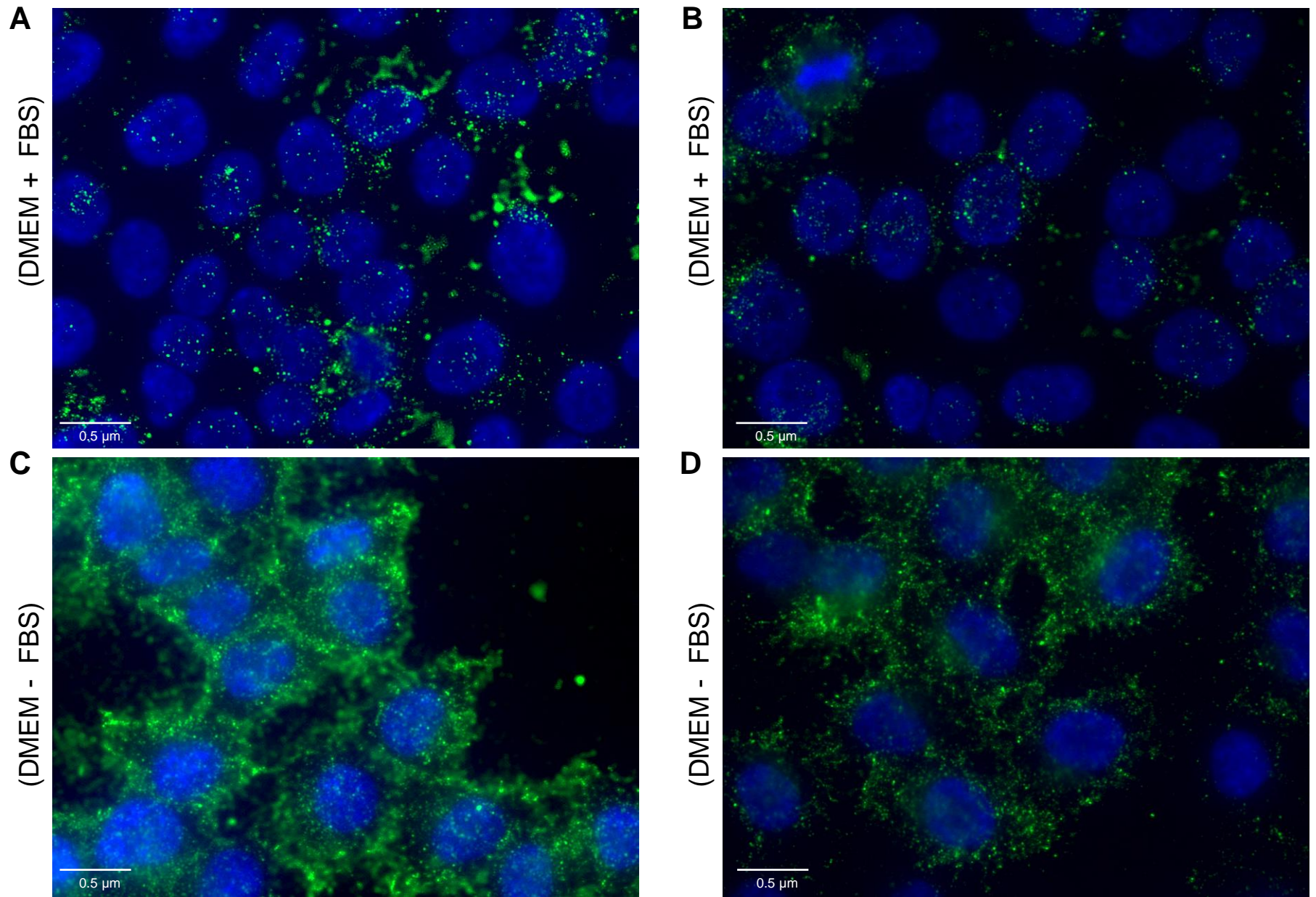
Supplementary Figure 3. Ascertaining G4-form specificity of BG4 antibody. **A.** Gel image of resolved radiolabelled *Hif1α* oligomeric substrate, RT17 (lanes 1-8). The marked bands were excised and eluted, followed by BG4 incubation at 4°C. **B.** Bound DNA (indicated by an arrow) was then electrophoresed on 6% native polyacrylamide gel.



Supplementary Figure 4. BG4-bound supercoiled plasmids. **A.** pSXneo135s shift substantially (lanes 1-4), unlike the control plasmid pSV4 (lanes 9-12), when electrophoresed for longer period (5 h vs 3 h). **B.** Bar diagram showing quantification of shift in mobility of supercoiled forms upon BG4 addition (0.00, 1.5, 2.3, 3 μg). 'Y' axis denotes the mobility shift of supercoiled form.



Supplementary Figure 5. Immunofluorescence imaging in Nalm6 with anti-RAG1 antibody. RAG1 antibody is added as a control in Nalm6 to check for foci formation. Cells were fixed in 2% paraformaldehyde and permeabilized with 0.1% Triton-X100, followed by blocking. Immunofluorescence was performed by incubating cells with RAG1 antibody at 4°C, followed by anti-rabbit secondary antibody. Following streptavidin-FITC incubation, coverslips were mounted with DABCO/DAPI and images were recorded by Zeiss Apotome. Nuclei were counterstained with DAPI (blue). RAG1 antibody was observed in FITC channel (green). First row is secondary control. Second and third rows are RAG1 antibody controls. Unlike the foci formation for BG4, RAG1 showed fluorescent background throughout the nucleus.



Supplementary Figure 6. BG4 foci in HeLa during nutrition-proficient and -deficient state. **A, B.** Majority of BG4 binds to nuclear G4 structures in HeLa under normal, serum-provided state, with marginal cytoplasmic signal. **C, D.** Serum starvation of cells for 48 hours, followed by BG4 staining, indicates more cytoplasmic localization of the antibody, with significantly lower nuclear foci.